Description of Three-Phase Filtration with a Novel Dimensionless Number

P. Huizenga, J. A. M. Kuipers, and W. P. M. van Swaaij
Dept. of Chemical Engineering, Twente University of Technology, 7500 AE Enschede, The Netherlands

Internal filtration in slurry bubble columns offers a possible solution to the filtration problems related to this reactor type. The applicability of the concept has already been demonstrated at full-scale for wastewater treatment, even though a theoretical description of internal filtration is lacking. Two types of hydrodynamic models were developed for a filtering slurry reactor. Both the model of the surface renewal type and the model based on a force-balance approach predict that the solids concentration at the axial position of the filter uniquely depends on a single novel dimensionless number. The validity of these theories was demonstrated by measuring filter-cake resistance as an indirect measure of solids concentration for a system in batch operation with respect to solids. In the experiments the load of solids, permeate flux (J), superficial gas velocity (U_g), particle diameter (d_p), kinematic liquid viscosity (υ_l), and molar mass of the gas were varied.

Introduction

In the chemical and process industries a wide variety of applications of slurry bubble columns can be found. In this reactor type a gas, a liquid, and a solid are brought into intense contact. The small particles (< 200 μm) applied are kept in suspension solely by the turbulence induced by the rising gas bubbles. A strong point of slurry reactors is their excellent heat-transfer characteristics, which explains their frequent use in processes involving strongly exothermic hydrogenation and oxidation reactions. The reduction of both internal and external diffusion resistances accomplished by using relatively small particles also constitutes a considerable advantage of slurry reactors. Often the solid phase acts as a catalyst and needs to be separated from a liquid product. External filtration implies displacement of the slurry and exposure of the solid catalyst to alternating conditions. The former is a strenuous operation, while the latter may lead to catalyst deactivation. These disadvantages can be avoided by performing internal filtration.

In sewage sludge treatment internal filtration has successfully been applied at commercial scale (Ishida et al., 1993; Kraft and Mende, 1995). The novel technology, originally developed in Japan by the Kubota Corporation, offers the possibility of operating at higher solids concentrations, which results in considerable reduction of reactor size. Furthermore, the sweeping action of the rising gas bubbles strongly reduces membrane fouling. Some patents (Rytter et al., 1994; Jager et al., 1994) concerning application of internal filtration to Fischer–Tropsch synthesis have appeared. In both patents cake breakdown by gas-flow-driven turbulence is claimed to facilitate slurry filtration.

When applying internal filtration, cake buildup leads to a less effective utilization of the slurry bulk and therefore needs to be prevented. If the solid phase acts as a catalyst cake buildup may also lead to hot-spot formation, possibly causing catalyst deactivation and product decomposition. To the knowledge of the authors no detailed hydrodynamic studies describing cake buildup in three-phase filtration have appeared in the literature. In this article the physical properties and operating conditions relevant to cake buildup and their respective influences are determined.

Three-Phase Filtration Models

In the rectangular system considered throughout this article (Figure 1a) gas and liquid are injected simultaneously at the bottom. Gas leaves the column at the top, while liquid is drained through the permeable sides of the filter zone. A certain weighted amount of particles is contained in the column, that is, the system operates in batch with respect to solids. In the axial direction solid-phase distribution is influ-

Correspondence concerning this article should be addressed to P. Huizenga.

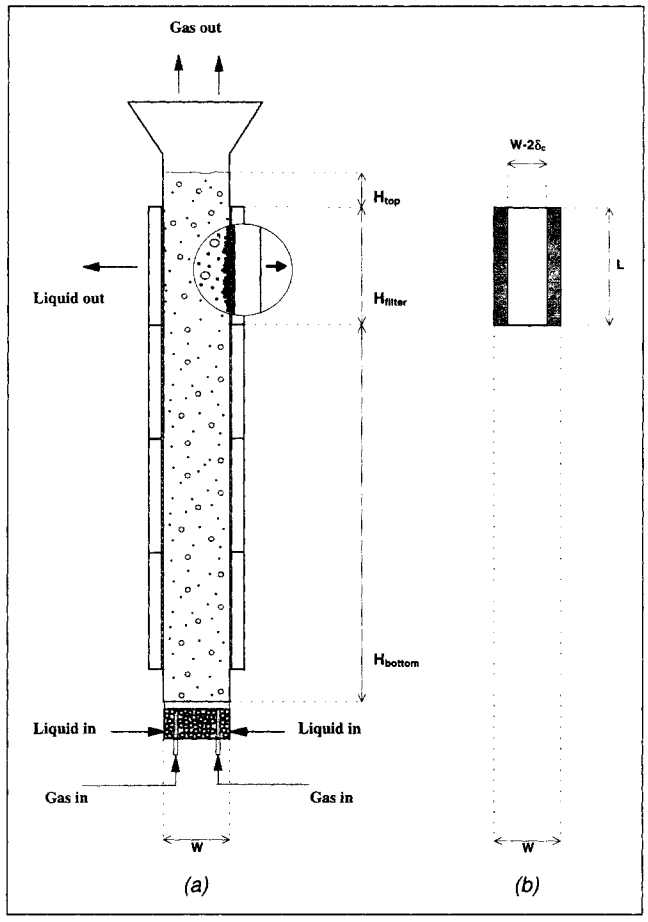

Figure 1. Filtering slurry bubble column used in the experiments: (a) front view of the column; (b) top view of the filter zone.

enced by net upward liquid convection (if present), sedimentation due to the density difference between solids and liquid, and dispersion caused by gas-induced liquid motion. There is no net flow of liquid in the region above the filter (top zone), since all entering liquid leaves the column through the permeable sides. In the filter zone particles tend to advect to the filter with the permeating liquid, leading to cake buildup. Particles are, however, swept away from the filter due to gas-induced turbulence. Figure 2 gives an overview of the relevant transport mechanisms.

Axial distribution of the solid phase in a filtering slurry system is very similar to that in an ordinary slurry system. The present article therefore focuses on the description of the distribution of the solid phase in the radial direction. Two models that have been developed for this purpose are discussed. Since both models are partially based on Kolmogoroff's theory of local isotropic turbulence, the latter is discussed first.

As will become clear during the discussion of the radial models, their validation requires measurement of solids concentration. In the experiments performed this quantity is, however, not measured directly. Instead the resistance of the filter cake has been measured as a function of imposed conditions (U_g, J, d_p, υ_l) and load of solids ($M_{s,tot}$) and scaled by its maximum value for the same batch of solids. In this way

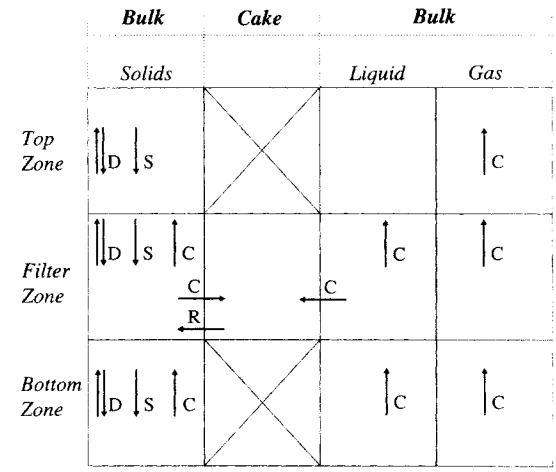

Figure 2. Overview of mechanisms relevant for the three phases present.

C = convection, D = dispersion, R = resuspension, S = sedimentation.

the so-called cake ratio (CR) is obtained, which is an indirect measure of solids concentration at the axial position of the filter under certain assumptions. Therefore at the end of this section models for radial and axial solids distribution are combined into models describing hydrodynamic behavior of the solid phase in the filtering slurry column considered in this article (Figure 1a). From the distribution of the solid phase in the system, the volume of solids present in the cake and therefore its resistance and the cake ratio can be calculated, allowing comparison of experimental and model results.

Kolmogoroff's theory of local isotropic turbulence

In slurry bubble columns Kolmogoroff's theory of local isotropic turbulence has successfully been applied for the description of liquid-to-solid mass transfer (see, e.g., Beenackers and van Swaaij, 1993) and wall-to-slurry heat transfer (Deckwer and Schumpe, 1985). Some objections have been raised against its application, however (Deckwer and Schumpe, 1985).

In a system in turbulent motion, macroscopic eddies are formed at the scale of the system itself. In bubble columns the formation of these large-scale eddies is induced by the motion of the rising gas bubbles. The macroscale eddies transfer kinetic energy to smaller-scale eddies. This process repeats itself until eddies of a certain scale dissipate kinetic energy into heat. If the Reynolds number exceeds a critical value, Kolmogoroff states that the universal equilibrium range exists (Hinze, 1975). The microscale eddies in this range then are responsible for the dissipation of kinetic energy from the system and behave isotropically, that is, they have lost any directional dependency. It is postulated that their behavior depends exclusively on energy dissipation rate per unit mass of liquid (E) and kinematic liquid viscosity (υ_l). From dimensional analysis, scales of length, velocity and time characteristic of energy-dissipating microscopic eddies can be deduced:

$$\lambda_k = \left(\frac{\upsilon_l^3}{E}\right)^{1/4} \tag{1}$$

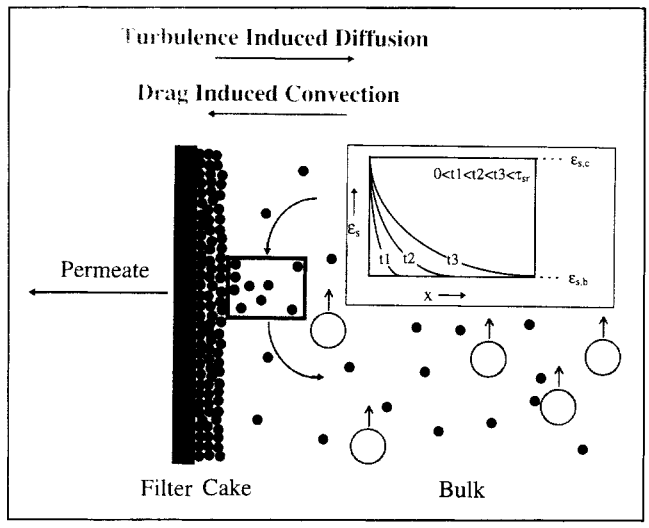

Figure 3. Surface-renewal model.

$$V_k = (\upsilon_l E)^{1/4} \tag{2}$$

$$\tau_k = \left(\frac{\upsilon_l}{E}\right)^{1/2}. \tag{3}$$

The Kolmogoroff length scale can be seen as the size of the smallest eddies present in the system (Hinze, 1975).

Surface-renewal model

Higbie's surface-renewal theory was successfully applied by Deckwer (1980) to describe wall-to-bulk heat transfer in bubble columns. For the exchange of particles between the slurry bulk and a filter cake, a similar approach can be undertaken. Small fluid elements remain at the cake surface for a certain contact time, after which they are replaced and remixed into the slurry bulk (Figure 3). During their stay at the cake surface unsteady convection and diffusion of particles occur, which can be described by

$$\frac{\partial \epsilon_s}{\partial t} = \frac{\partial}{\partial x}\left\{D_s \frac{\partial \epsilon_s}{\partial x} - \frac{J}{1-\epsilon_s}\epsilon_s\right\}. \tag{4}$$

The necessary initial and boundary conditions are given by

$$t = 0, x \geq 0: \qquad \epsilon_s = \epsilon_{s,b} \tag{5}$$

$$t > 0, x = 0: \qquad \epsilon_s = \epsilon_{s,c} \tag{6}$$

$$t > 0, x > 0: \qquad \epsilon_s = \epsilon_{s,b}. \tag{7}$$

The system is at hydrodynamic equilibrium if the time-average flux of particles at the cake surface ($x = 0$) during the residence time τ_{sr} equals zero. Another way to express the equilibrium condition is that the net accumulation of particles in the liquid elements after their stay equals the amount entered from the slurry bulk by convection:

$$t = \tau_{sr}: \qquad \int_0^\infty (\epsilon_s - \epsilon^*_{s,b})\, dx = \frac{J}{(1-\epsilon^*_{s,b})}\epsilon^*_{s,b}\tau_{sr}. \tag{8}$$

Table 1. Closure equations of the Surface-Renewal Model

$\tau_{sr} = C_\tau \tau_{k,sl} = \dfrac{400}{\pi}\sqrt{\dfrac{\upsilon_{sl,b}}{E}}$	
$\upsilon_{sl,b} = \upsilon_l \dfrac{1+4.5\epsilon_{s,b}}{1+\left(\dfrac{\rho_s}{\rho_l}-1\right)\epsilon_{s,b}}$	Deckwer et al. (1980)
$E = U_g g$	
$D_s = \epsilon_s^2\left(1-\dfrac{\epsilon_s}{\epsilon_{s,c}}\right)\dfrac{\sigma_x}{\eta_l}\dfrac{1}{4}d_p^2$	Chapman and Leighton (1991)
$\sigma_x = \eta_{sl,b}\dot{\gamma}_{sl,b} = (1+4.5\epsilon_{s,b})\eta_l \dfrac{C_\sigma}{\tau_{k,sl}}$	

The surface-renewal model requires closures for the residence time τ_{sr} and the diffusion coefficient D_s. For the first quantity an expression can be deduced from the description of heat transfer in slurry bubble columns proposed by Deckwer et al. (1980). These authors showed that the relationship derived by Deckwer (1980) also holds for slurry bubble columns, provided that the physical properties of the liquid are replaced by mixture properties of the slurry (Table 1). In their approach the residence time is set proportional to the Kolmogoroff time scale, assuming that microscale eddies are responsible for radial mixing.

Shear induced diffusion has been shown to be the main mechanism responsible for particle resuspension in laminar crossflow microfiltration of particles in our size range (Davis, 1992). Under the influence of shear, particles will diffuse toward regions of lower viscosity and solids concentration. The shear-induced diffusion coefficient has been measured by Chapman and Leighton (1991) and by Leighton and Acrivos (1986). The best fit given by Chapman and Leighton is used here in a simplified form as a closure for the diffusion coefficient D_s (Table 1). The unknown shear stress can be calculated, assuming that the characteristic shear rate is proportional to the reciprocal of the Kolmogoroff time scale. This seems to be a reasonable assumption, if particle resuspension from the filter cake can be attributed to the microscale eddies. The unknown proportionally constant C_σ needs to be fitted from experimental data.

After substitution of the equations given for residence time and diffusion coefficient, the following dependency holds for the equilibrium solids bulk concentration:

$$\epsilon^*_{s,b} = f\left(\frac{J}{d_p}\sqrt{\frac{\upsilon_l}{U_g g}}, \frac{\rho_s}{\rho_l}, \epsilon_{s,c}\right). \tag{9}$$

The density ratio enters the equation through the kinematic slurry viscosity (Table 1). It is expected to be of minor importance for slurries containing only a few volume percent of solids as used in our experiments (Table 2). If the solids holdup in the cake is further considered to be constant, it follows that the equilibrium solids concentration in the slurry is given by

$$\epsilon^*_{s,b} = f\left(\frac{J}{d_p}\sqrt{\frac{\upsilon_l}{U_g g}}\right) = f(\Pi_{sr}). \tag{10}$$

Table 2. Range of Experimental Conditions*

Variable	U_g [cm/s]	J [mm/s]	U_l [cm/s]	d_p [μm]	ν_l [10^{-6} m^2/s]	T [°C]	M_s [g]	$\epsilon_{s,avg}$ [%]
Min.	0.50	0.83	0.77	41	0.66	10	15.0	0.70
Max.	3.50	2.15	2.00	96	1.31	40	60.0	2.82

*Quantities relevant to cake buildup number in italic. $\epsilon_{s,avg}$ = solids volume/total G/L/S slurry volume.

Thus the model predicts the existence of an equilibrium solids concentration, which should depend on a single dimensionless number.

Though this model cannot be solved analytically for the general case of varying $\epsilon^*_{s,b}$, a limiting solution can be derived that is valid for the solids concentration range considered (see the Appendix). This limiting solution is applied in the model to be discussed in the subsection titled "Filtering-Slurry Bubble-Column Model."

Strictly speaking, shear-induced diffusion is a phenomenon occurring under laminar conditions. Therefore the approach followed here seems rather crude. An alternative is offered by the force-balance model, which we discuss next.

Force-balance model

Consider a single particle at the axial position of a filter in a three-phase system. Due to permeate flow, the particle experiences a drag force, which for particles in the Stokes regime can be written as

$$F_D = 3\pi\eta_l d_p J f(\epsilon_{s,b}). \tag{11}$$

The equation of Wen and Yu (1966) is used to correct the drag force acting on an isolated particle for the presence of other particles.

$$f(\epsilon_{s,b}) = (1-\epsilon_{s,b})^{-4.7}. \tag{12}$$

The drag force exerted on the particle by the permeate flow is counteracted by the resuspension force caused by turbulent eddies:

$$F_R = \frac{1}{4}\pi d_p^2 \rho_l (V')^2. \tag{13}$$

For the fluctuation velocity of the relevant eddies, Davies (1972) gives, for a pure fluid,

$$V' = (E\lambda)^{1/3}. \tag{14}$$

This equation was derived for medium-scale eddies, which are assumed insensitive with respect to fluid viscosity. For microscale eddies, substitution of the Kolmogoroff length scale leads to the Kolmogoroff velocity scale.

Locally, turbulence is damped due to the presence of the particles. Following Davies (1986) we correct for this phenomenon in a simple manner, since no quantitative knowledge is available at present:

$$V' = \frac{(E\lambda)^{1/3}}{1+\alpha\epsilon_{s,b}}. \tag{15}$$

At hydrodynamic equilibrium the two forces balance each other, which leads to

$$\frac{J\nu_l}{d_p(E\lambda)^{2/3}} = \frac{1}{12 f(\epsilon^*_{s,b})(1+\alpha\epsilon^*_{s,b})^2}. \tag{16}$$

The choice of the length scale of the resuspending eddies is by no means trivial. Davies (1986, 1987) was able to describe resuspension both in horizontal pipe flow and stirred tanks, assuming that particle diameter is the relevant length scale. Bearing in mind the relevance of microscale eddies in connection with radial dispersion, the Kolmogoroff length scale might also be a good option. A third option is to connect the length scale of the resuspending eddies to the diameter of the bubbles, since their motion acts as the source of turbulence in our system. For reasons of simplicity a direct proportionality might be assumed.

Depending on the length scale chosen, the equilibrium condition can now be rewritten in the following general form:

$$\Pi_{fb} = \frac{1}{12 f(\epsilon^*_{s,b})(1+\alpha\epsilon^*_{s,b})^2}\left(\frac{\nu^*_{sl,b}}{\nu_l}\right)^a \tag{17}$$

$$\lambda = C_b d_b: \quad \Pi_{fb} = \frac{J\nu_l}{d_p(C_b d_b)^{2/3}(U_g g)^{2/3}}, \quad a = 0$$

$$\lambda = d_p: \quad \Pi_{fb} = \frac{J\nu_l}{d_p^{5/3}(U_g g)^{2/3}}, \quad a = 0$$

$$\lambda = \lambda_k: \quad \Pi_{fb} = \frac{J\sqrt{\nu_l}}{d_p\sqrt{U_g g}}, \quad a = \frac{1}{2}.$$

In all three cases considered the force-balance model also leads to a single dimensionless number that determines the equilibrium value of solids bulk concentration. *Note that upon choosing the Kolmogoroff length scale, the force-balance model and the penetration model even result in the same dimensionless number.* In this case the weak dependency on the density ratio also reappears (Eq. 17; Table 1), which can be neglected based on the arguments mentioned in the previous subsection.

In the dimensionless number of relevance, gas velocity, particle diameter, and kinematic liquid viscosity possess different exponents for different choices of λ. Therefore no selection is made at this point and it is left up to experiment to decide on the correct magnitude of the resuspending eddies.

Filtering-slurry bubble-column model

Either of the two models discussed in the previous sections can now be embedded in a model describing hydrodynamics

of the rectangular filtering-slurry bubble column used in the experiments (Figure 1). This column is equipped with two filters in parallel at a certain axial position, where depending on imposed conditions (U_g, J, d_p, v_l) and load of solids ($M_{s,\mathrm{tot}}$) a cake of particles may form. In the experiments performed the resistance of the cake is measured and scaled by its maximum value for the same batch of solids. In this way the so-called cake ratio is obtained, which is an indirect measure for solids concentration at the axial position of the filter under certain assumptions. In the model cake resistance follows from the Kozeny–Carman equation, assuming that a uniform cake is formed on the filter:

$$R_c = \bar{R}_c \delta_c = 180 \frac{\epsilon_{s,c}^2}{(1-\epsilon_{s,c})^3} \frac{1}{d_p^2} \delta_c. \tag{18}$$

Maximum cake thickness for a uniform cake can be calculated from the load of solids:

$$\delta_{c,\max} = \frac{M_{s,\mathrm{tot}}}{\rho_s \epsilon_{s,c}} \frac{1}{2LH_{\mathrm{filt}}}. \tag{19}$$

Therefore, for a uniform cake it holds:

$$\mathrm{CR} = \frac{R_c}{R_{c,\max}} = \frac{\delta_c}{\delta_{c,\max}} = \frac{M_{s,c}}{M_{s,\mathrm{tot}}} = \frac{V_c^s}{V_{\mathrm{tot}}^s} = \frac{V_{\mathrm{tot}}^s - V_b^s}{V_{\mathrm{tot}}^s}. \tag{20}$$

For a uniform bulk its solids content is directly proportional to solids concentration in the vicinity of the filter as determined by one of the two radial models. In this case in the model calculations cake ratio is a measure for solids concentration, since it is by definition a measure for solids content in the slurry bulk (Eq. 20). In our model axial nonuniformities are accounted for by the well-accepted sedimentation-dispersion model. From the model calculations we will examine the extent to which radial effects dominate the influence of axial concentration gradients.

Cake thickness at equilibrium for a specific set of imposed conditions (U_g, J, d_p, v_l) and load of solids ($M_{s,\mathrm{tot}}$) is determined iteratively. For an arbitrary cake thickness and a certain set of imposed conditions, the mass of solids that would be present in the column at equilibrium can be calculated from the model, as is discussed later. If this value exceeds the load of solids present in the system, the equilibrium thickness is less than its present value, while in the opposite case equilibrium thickness exceeds its present value. In the model calculations cake thickness at equilibrium is determined by bisection at the interval $[0, \delta_{c,max}]$ with a relative accuracy of 10^{-6} with respect to interval width.

In the calculation of the equilibrium mass of solids the column is subdivided in a region below the filters (bottom zone), a region at the height of the filters (filter zone), and a region above the filters (top zone):

$$M_s^* = M_{s,b,\mathrm{bottom\,zone}}^* + M_{s,c} + M_{s,b\,\mathrm{filter\,zone}}^* + M_{s,b,\mathrm{top\,zone}}^*. \tag{21}$$

In the filter zone axial variations are neglected and solids concentration ($\epsilon_{s,b}^*$) is determined either by the surface-renewal model (Eq. A1) or the force-balance model (Eq. 17). Due to cake formation cross-sectional area may be reduced (Figure 1b), leading to a higher superficial gas velocity in this region:

$$U_{g,\mathrm{filter\,zone}} = \frac{U_g}{a_b} \tag{22}$$

$$a_b = \frac{W - 2\delta_c}{W}. \tag{23}$$

The equilibrium mass of solids that can be present in the bulk of the filter zone for a certain cake thickness then follows from the equilibrium value of solids concentration (Table 3). In this calculation solids holdup in the slurry bulk is multiplied by slurry holdup, $(1-\epsilon_g)$, to obtain solids volume fraction based on the volume of the three phases present. The required value for gas holdup is obtained from the equation given by Darton (1984) (Table 4).

Knowledge of the solids concentration profile in the regions above and below the filter zone is required for deter-

Table 3. Expressions for Solids Content in the Filter Cake and in the Bulk of the Three Zones

$M_{s,b,\mathrm{bottom\,zone}}^* = \rho_s \epsilon_{s,b}^*(1-\epsilon_{g,\mathrm{bottom\,zone}}^*)WL \frac{1}{C_{\mathrm{bottom}}^*}(e^{C_{\mathrm{bottom}}^* H_{\mathrm{bottom}}} - 1)$ $C_{\mathrm{bottom}} = \frac{V_p - V_l}{D_{\mathrm{ax},s}}$
$M_{s,c}^* = \rho_s \epsilon_{s,c} LH_{\mathrm{filter}} W(1-a_b^*)$
$M_{s,b,\mathrm{filter\,zone}}^* = \rho_s \epsilon_{s,b}^*(1-\epsilon_{g,\mathrm{filter\,zone}}^*)LH_{\mathrm{filter}} W \quad a_b^*$
$M_{s,b,\mathrm{top\,zone}}^* = \rho_s \epsilon_{s,b}^*(1-\epsilon_{g,\mathrm{top\,zone}}^*)WL \frac{1}{C_{\mathrm{top}}^*}(1-e^{-C_{\mathrm{top}}^* H_{\mathrm{top}}})$ $C_{\mathrm{top}} = \frac{V_p}{D_{\mathrm{ax},s}}$

Table 4. Closure Equations of the Continuously Filtering Slurry Bubble-Column Model

$\epsilon_g = \frac{1}{8}\ln\left(1+1.6g^{-7/24}\left(\frac{\eta_{sl,\mathrm{Darton}}}{\rho_{sl}}\right)^{1/6}\left(\frac{\omega}{\rho_{sl}}\right)^{-1/8} U_g\right)$ Darton (1984) $\eta_{sl,\mathrm{Darton}} = \eta_l e^{36.15\epsilon_{s,b}^{2.5}}$ $\rho_{sl} = \epsilon_{s,b}\rho_s + (1-\epsilon_{s,b})\rho_l$
$Pe_s = 13Fr_g \frac{(1+0.009Re_t Fr_g^{-0.8})}{1+8Fr_g^{0.85}}$ Kato et al. (1972) $V_p = 1.33\, V_t^{0.75} U_g^{0.25}(1-\epsilon_{s,b})^{2.5}$ $V_t = \frac{(\rho_s - \rho_l)gd_p^2}{18\eta_l}$

mining the equilibrium mass of solids that could be present there. A sedimentation-dispersion (SD) model (Cova, 1966) is applied for this purpose. Since the experiments were performed in batch mode with respect to solids, the SD model can be reduced to

$$D_{\mathrm{ax},s}\frac{\partial \epsilon_{s,b}}{\partial z}-(V_l-V_p)\epsilon_{s,b}=0. \tag{24}$$

Sedimentation velocity and axial dispersion coefficient are calculated according to Kato et al. (Table 4).

Bearing in mind that at the bottom of the top zone ($z=0$) solids concentration equals its value in the filter zone ($\epsilon^*_{s,b}$), the SD model can be solved to give the solids concentration profile in this region:

$$\epsilon_{s,b}(z)=\epsilon^*_{s,b}e^{-C^*_{\mathrm{top}}z};\qquad C_{\mathrm{top}}=\frac{V_p}{D_{\mathrm{ax},s}}. \tag{25}$$

The equilibrium mass that could be present in the top zone then follows by integration (Table 3). In the derivation of the these results, sedimentation velocity and gas holdup are assumed to be independent of height, which is allowed since applied slurry concentrations are low (Table 2). A similar procedure is followed for the bottom zone.

The model discussed in this section is dedicated to the setup used in this work. The approach followed can, however, be applied to any filtering slurry system. Moreover, it should be emphasized that the models describing radial distribution of the solid phase discussed in the two previous sections have a general validity. Their inclusion in the filtering-slurry bubble-column model is only required to allow their validation by the experiments performed.

Equipment and Experimental Procedure

The experiments were performed in a rectangular Perspex slurry bubble column ($W=25$ mm; $L=50$ mm) possessing filters 488 mm in length on two parallel sides 40 mm distant from the bottom (Figure 1). The top section of the column consists of a cone with a removable cover. The filters consist of $325\times2{,}300$ mesh stainless-steel wire gauze attached to a perforated plate ($d=2$ mm) using double-sided adhesive tape 0.09 mm thick. In the axial direction the permeable area was divided into four equally sized parts by dams 8 mm high, leaving a 116×50 mm^2 permeable area per part. Each part had its own collection compartment equipped with a liquid outlet at the bottom, a pressure indication point at half-height, and a deaeration outlet at the top. At the half-height of each compartment the back wall of the column contained pressure indication points covered with $165\times1{,}400$ mesh wire gauze to prevent solids discharge from the column. For the same reason the bottom of the column was covered with $325\times2{,}300$ mesh wire gauze, supported on top using a perforated plate ($d=1$ mm). In the experiments reported in this study only the left and right top compartments were used ($H_{\mathrm{bottom}}=412$ mm; $H_{\mathrm{filter}}=116$ mm).

In Figure 4 a flow scheme of the experimental setup is shown. Mass flow controllers (Brooks, type 5850 TR) were used to provide for equal gas distribution through the six gas

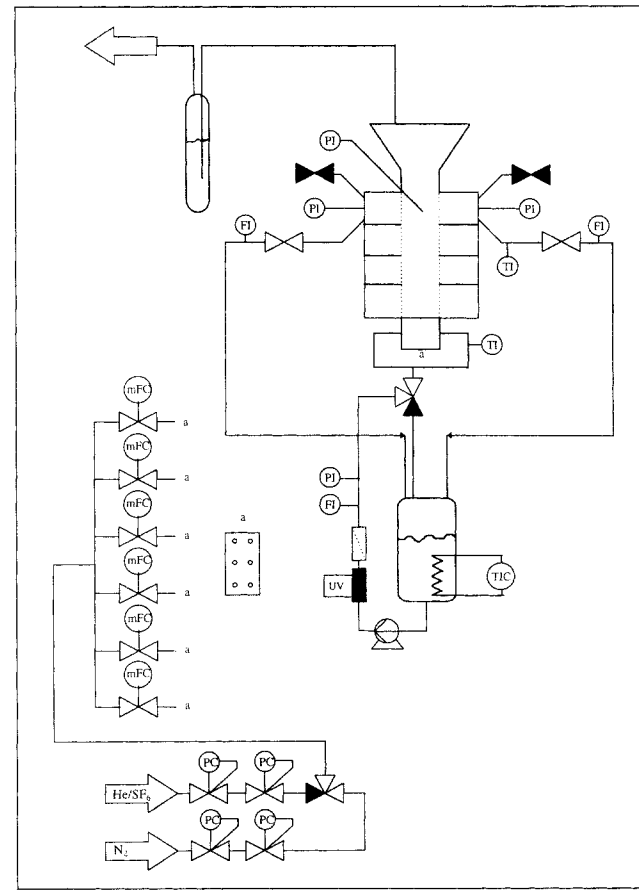

Figure 4. Experimental setup.

injection tubes ($d=1$ mm) of the column. Gas leaving the column passed through a water lock to enable pressure control. In our study helium (He), nitrogen (N_2), and sulphur hexafluoride (SF_6) were used as gaseous media. A pump, equipped with a frequency controller, continuously fed demineralized water from a storage vessel to a PURA ultraviolet disinfection/active carbon filtration system, followed by a depth filter. Prior to entering the column, water passed through a rectangular packed bed 50 mm high consisting of 2.5-mm glass spheres surrounding the gas-injection tubes. For each compartment water flow rate from the column to the storage vessel was controlled with a Brooks Rotameter. A weighed amount (15–60 g) of glass beads ($\rho_s=2{,}890$ kg·m^{-3}) possessing narrow size distributions could be added to the column by the conical top section. The volume average diameters of the applied batches of solids were 41, 42, 57 and 96 μm, respectively.

Experiments were performed both in the absence and the presence of particles. The resistance due to cake-layer formation could be determined from the difference in resistance to filtration between both cases. In the experiments in an unloaded system, that is, in the absence of particles, liquid temperature and flow rates of liquid and gas were set to the desired values. Liquid temperature was controlled by pumping water from a thermostatic bath through a spiral submerged in the liquid storage vessel. Liquid temperature (viscosity) was measured just before the injection and at the top right outlet. Pressure drops were measured applying manometers with a

common enclosed gas cap using water from the column as manometer liquid. To increase measurement accuracy the manometers were mounted under an angle of 30° with respect to the horizontal.

In the experiments with particles present the liquid temperature and flow rate and gas flow rate were set first. Then the level of the gassed slurry was adjusted to 589 mm (H_{top} = 61 mm) by manipulating the rotameter valves and, if necessary, column pressure. Care was taken to keep the flow rates of the effluent equal on both sides. When the system seemed to stabilize, any filter cake that might be present was destroyed by setting gas velocity equal to 3.5 cm/s and temporarily blocking liquid outflow. Then the gas velocity was gradually reduced to its desired value. If necessary, the rotameter valves were slightly adjusted to keep the steady-state slurry level constant. Finally, the flow rates of liquid and gas, liquid temperature (viscosity), and determined pressure drops were recorded. The range of experimental conditions studied is reported in Table 2.

Results and Discussion

Filter resistance

Prior to adding particles to the system, filter resistance (R) was determined using Darcy's law:

$$R = \frac{\Delta p}{\eta_l J}. \tag{26}$$

This quantity was shown to be independent of liquid flow rate, gas velocity, and temperature. For several reasons (e.g., fouling) filter resistance may change in the course of time. Filter resistance was therefore checked on a daily basis after particles had been added to the system. Four measurements spanning the full range of gas and liquid flow rates were reproduced. If necessary, filter resistance was corrected based on these measurements.

Reproducibility and symmetry

For each set of operating conditions the total resistance to filtration was calculated from Darcy's law for both compartments. Subsequently, cake resistances were determined by subtracting the respective filter resistances from the total filtration resistances. When the flow rates of both compartments were allowed to deviate by 10% while keeping total flow constant, the left and right cake resistances differed by a factor of 2 or more. However, average of the cake resistance of both sides then only changed by 3% and was therefore considered a reliable measure for cake resistance at a certain average permeate flux. Reproducibility was found to be well within 3%, except for very low cake resistances where errors up to 20% were observed.

Maximum resistances

For the particle sizes and loads of solids listed in Table 2 the maximum cake resistance was determined by setting the gas flow rate to zero, while setting the liquid flow rate to its maximum value. Maximum resistance was proven to be directly proportional to the load of particles and inversely proportional to the square of Sauter mean particle diameter. Assuming a cake solidity of 0.63 and a uniform cake, all measured maximum resistances could be described well by the Kozeny–Carman equation.

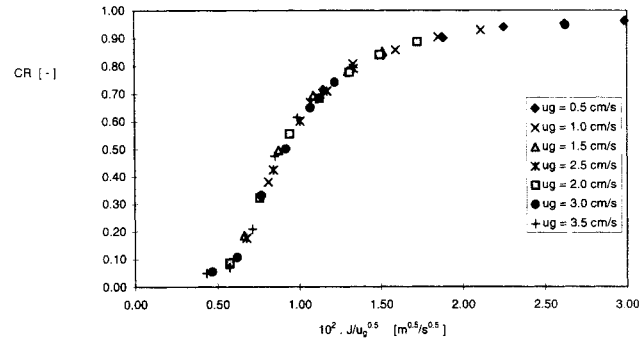

Figure 5. Experimental results for simultaneous variation of gas velocity and permeate flux.

Results are plotted assuming the exponent of gas velocity to be $-1/2$; 30-g glass beads, $d_p = 41$ μm, $T = 29$°C, gas = N_2.

Cake ratio

To allow direct comparison of the experiments performed for different particle sizes, the cake resistance was scaled by its maximum value to obtain a dimensionless quantity termed the cake ratio. In case the resistance of the cake is a monotonically increasing function of the cake volume, this quantity represents an indirect measure of the volume of solids contained in the slurry bulk. If volume of solids in the slurry bulk is an increasing function of solids concentration at the axial position of the filter, cake ratio can be seen as an indirect measure for the latter and should therefore depend on the same dimensionless number. These conditions are the weakest that can be formulated for cake ratio being a measure for solids concentration and are considerably less stringent than those mentioned in the subsection on the filtering-slurry bubble-column model.

Influence of gas velocity

In Figures 5 and 6 results of experiments are shown in which gas velocity and permeate flux were varied simultane-

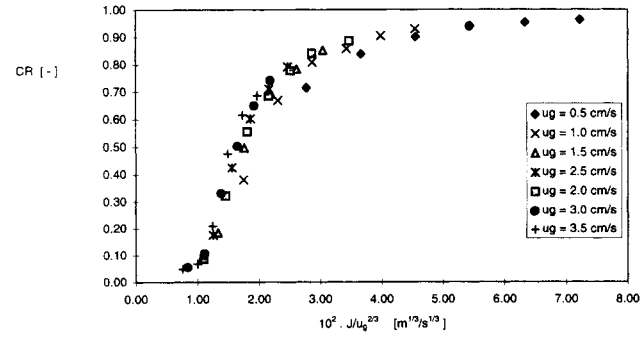

Figure 6. Experimental results for simultaneous variation of gas velocity and permeate flux.

Results are plotted assuming the exponent of gas velocity to be $-2/3$; 30-g glass beads, $d_p = 41$ μm, $T = 29$°C, gas = N_2.

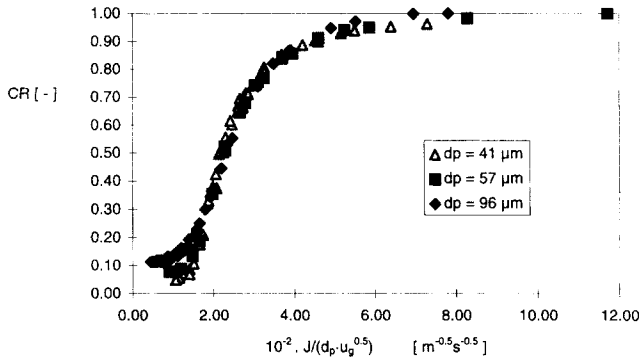

Figure 7. Experimental results for simultaneous variation of gas velocity, permeate flux, and particle diameter.

Results are plotted assuming the exponent of particle diameter to be -1: 30-g glass beads, $T = 29°C$, gas $= N_2$.

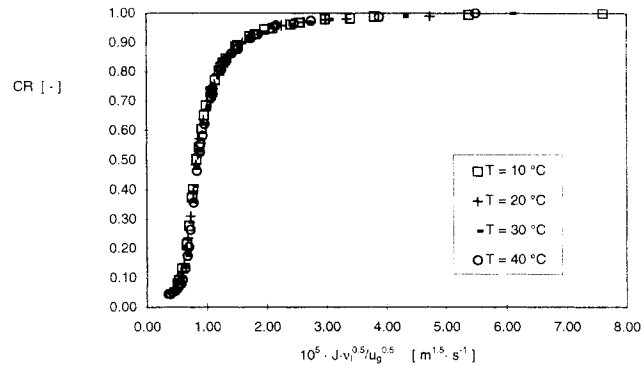

Figure 9. Experimental results for simultaneous variation of gas velocity, permeate flux, and temperature.

Results are plotted assuming the exponent of kinematic liquid viscosity to be $+1/2$: 30-g glass beads, $d_p = 41$ μm, gas $= N_2$.

ously. As evident from Figure 5, measured cake ratios can be described well by a single curve, assuming the exponent of gas velocity is $-1/2$. On the left side of the curve the cake ratio assumes low values, implying almost complete particle suspension, while on the right side of the curve the cake ratio approaches 1, implying that all particles have moved into a cake. The residual resistance on the left side of the curve can be attributed to the geometry of the filter. Even though on average turbulence is able to resuspend the particles, at the position of the holes of the carrier plate, liquid velocity may be higher than permeate flux for low cake ratios, leading to the formation of a small cake. In the dimensionless numbers derived, the only exponents occurring for gas velocity are $-1/2$ and $-2/3$. Supposing the gas-velocity exponent is $-2/3$, the unique dependency of the cake ratio is no longer observed (Figure 6).

Influence of particle diameter

From Figure 7 it can be seen that experimentally determined cake ratios fall on a single curve, assuming an exponent -1 for particle diameter. Assuming that the particle diameter is the length scale characteristic to the resuspending eddies, an exponent $-5/3$ was derived from the force-balance theory. Taking this value for the exponent of particle diameter, clearly no unique dependency of cake ratio is observed (Figure 8). The dimensionless number based on the particle diameter as the characteristic length scale should therefore probably be rejected.

Influence of liquid kinematic viscosity

The results of experiments in which permeate flux, gas velocity, and temperature were varied are shown in Figures 9 and 10. Taking an exponent $+1/2$ for liquid kinematic viscosity, measured cake ratios can be described by a single curve (Figure 9). When the length scale characteristic of the resuspending eddies was assumed to be proportional to bubble diameter or equal to particle diameter, an exponent $+1$ for viscosity was found. Clearly no unique dependency of cake ratio is found for this value of the exponent (Figure 10). The dimensionless numbers based on particle diameter and a quantity proportional to bubble diameter as the length scale characteristic of the resuspending eddies should therefore be rejected.

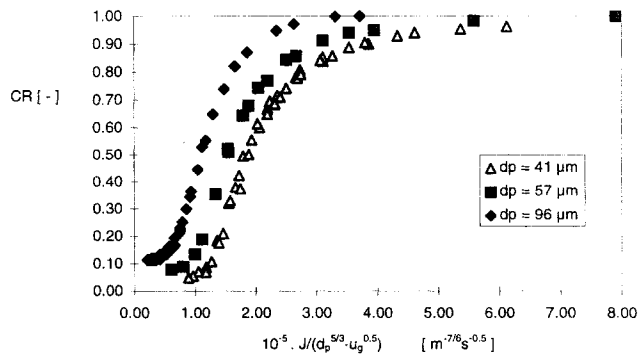

Figure 8. Experimental results for simultaneous variation of gas velocity, permeate flux, and particle diameter.

Results are plotted assuming the exponent of particle diameter to be $-5/3$: 30-g glass beads, $T = 29°C$, gas $= N_2$.

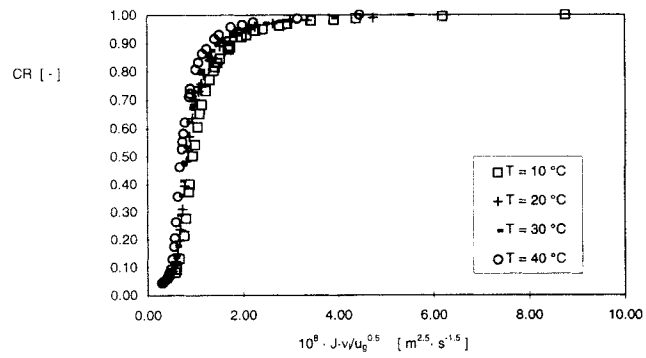

Figure 10. Experimental results for simultaneous variation of gas velocity, permeate flux, and temperature.

Results are plotted assuming the exponent of kinematic liquid viscosity to be $+1$: 30-g glas beads, $d_p = 41$ μm, gas $= N_2$.

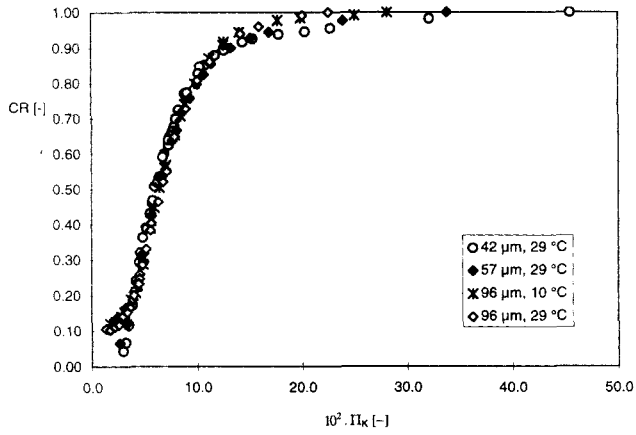

Figure 11. Experimental results for simultaneous variation of gas velocity, permeate flux, particle diameter, and temperature.

60-g glass beads, gas = N_2.

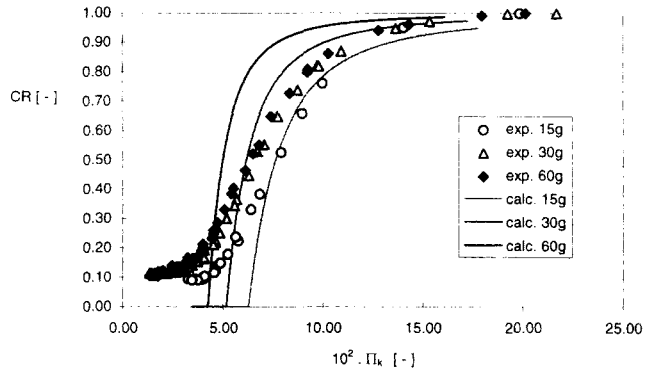

Figure 12. Experimental and surface-renewal model ($C_\sigma = 1.40$) results for simultaneous variation of gas velocity, permeate flux, and load of solids.

The dimensionless number has been corrected for cross sectional area reduction (Eq. 22): $d_p = 96$ µm, $T = 29$°C, gas = N_2.

Dimensionless number

From the foregoing it can be seen that for 15 g of particles, only one of the dimensionless numbers derived shows a unique relationship with the cake ratio. Similar results were obtained for 30 and 60 g of beads (Figure 11). The correct dimensionless number, hereafter called cake buildup number (Π_k), can be derived from the surface-renewal model as well as from the force-balance model provided that in the latter the Kolmogoroff scale is assumed to be the length scale of the resuspending eddies. Experimentally determined exponents are based on cake ratio measurements, however, and not on solids holdup measurements. Therefore the exponents found might have been influenced by axial effects. An indication of this influence can be obtained from model calculations and is discussed in more detail later.

Model predictions

The optimal values of the unknown constants in the force-balance model (α) and the surface-renewal model (C_σ) were determined by fitting the filtering-slurry bubble-column model to experiments for CR = 0.5 for each load of particles applied (Table 5). Since measured curves are at their steepest in this region, the dimensionless number corresponding to CR = 0.5 can be determined accurately. Note that the fitted damping factors are in the same order of magnitude as the values reported by Davies (1986).

From Table 5 it can be seen that depending on the load of solids, fitted values for the unknown constants vary by a factor of 2–2.5. These are only small variations if one considers the simplicity of the models applied. In Figures 12 and 13, respectively, the fitted cake ratio curves are shown for the surface-renewal model and the force-balance model at a solids load of 15 g. Except at low cake ratios, the surface-renewal model performs rather well, while the force-balance model results in a curve that is much steeper than the experimentally observed curve.

Knowing the value of C_σ, the ratio of penetration depth and particle diameter follows from Eq. A3. Since applied solids concentrations are low, viscosity and density of the slurry almost equal the properties of the liquid. It then follows that penetration depth and particle diameter are of the same order of magnitude for the experiments described, which renders the validity of the derivation of the surface-renewal model somewhat doubtful. The excellent descriptive qualities of the model, however, strongly plead in favor of its applicability.

According to both the surface-renewal model and the force-balance model, solids concentration at the axial position of the filter should uniquely depend on the cake buildup number. The same dependency does not necessarily hold for the cake ratios calculated from the filtering-slurry bubble-column model, however. Solids content of the slurry bulk, and

Table 5. Fitted Values for the Unknown Constants in the Force-Balance Model (α) and the Surface-Renewal Model (C_σ)

M_s [g]	15	30	60
α	4.0	10.0	5.0
C_σ	1.40	1.80	3.40

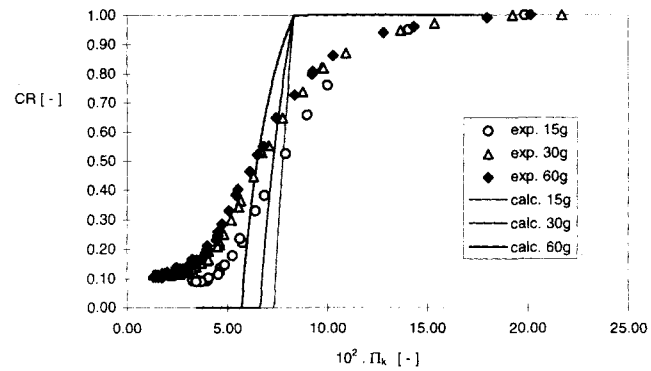

Figure 13. Experimental and force-balance model ($\alpha = 4.0$) results for simultaneous variation of gas velocity, permeate flux, and load of solids.

The dimensionless number has been corrected for cross-sectional area reduction (Eq. 22): $d_p = 96$ µm, $T = 29$°C, gas = N_2.

Table 6. Cake Buildup Number Exponents vs. Optimal Exponents Found Upon Substitution of the Two Radial Models Developed in the Filtering-Slurry Bubble-Column Model

	U_g	d_p	v_l
Force-balance model	−0.48	−0.985	0.485
Surface-Renewal model	−0.42	−0.88	0.42
Cake Buildup number	−0.50	−1.00	0.50

Base case: 15-g glass beads, $U_g = 0.5$ cm/s, $U_l = 0.77 - 2.00$ cm/s, $dp = 96$ μm, $T = 29$°C.

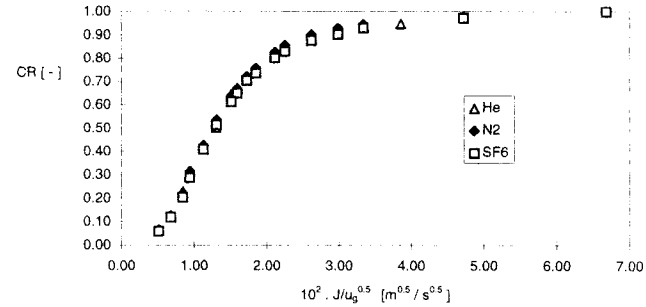

Figure 14. Experimental results for simultaneous variation of gas velocity, permeate flux, and molar mass of the gas.

Results are plotted assuming the exponent of gas velocity to be −1/2: 60-g glass beads, $d_p = 57$ μm, $T = 29$°C.

therefore cake ratio also depend on axial dispersion, sedimentation, and gas holdup. Cake-ratio curves were therefore calculated by varying permeate flux at a solids load of 15 g for different values of gas velocity, kinematic liquid viscosity, and particle diameter. Optimal exponents (a) were determined for the quantities (q) considered by letting the curves of cake ratio vs. $J \cdot q^a$ intersect in the vicinity of CR = 0.5. The exponents found compare quite well with the exponents in the cake buildup number (Table 6). Deviations found can be explained by the influence of superficial liquid velocity on the axial solids distribution. If permeate flux is increased to keep the cake buildup number constant compared to a certain reference state, superficial liquid velocity is also increased. This leads to a reduction of solids content in the bottom zone and thus to an increase in cake ratio.

Length scale of the resuspending eddies

Model calculations indicate only a minor influence of axial effects on the dimensionless number found. It can therefore be concluded from the experimentally validated dimensionless number that the resuspending eddies in our system can be characterized by the Kolmogoroff scales. For the resuspension in stirred tanks (Davies, 1986) and in horizontal pipe flow (Davies, 1987) it was shown, however, that the resuspending eddies are well characterized by the particle diameter as the characteristic length scale. This difference may be attributed to the ratio of particle diameter and Kolmogoroff length scale. In the experiments described in this article particle diameter was varied between 41 and 96 μm, while the Kolmogoroff length scale varies between 30 and 82 μm. While in our system the Kolmogoroff eddies are of the same order of magnitude as the particle diameter, this is not the case for the systems described by Davies. For the pipe flow system the particle diameter exceeds the Kolmogoroff scale by a factor ranging from 3 to 148, while a value of 50 is mentioned by the author as a typical ratio in the stirred-tank situation. Apparently particles are mainly influenced by eddies of a size comparable to their own, which is in agreement with the observations by Kuboi et al. (1972).

Influence of gas density

One might argue that in the previous discussions bubble diameter was assumed constant. If one would substitute the correct dependencies for the bubble diameter, the correct exponent for viscosity might appear. To overcome this deficiency, experiments were performed in which gas density was varied. It is well established from the literature that in a gas–liquid bubble column gas holdup increases and bubble diameter decreases with increasing gas density (Wilkinson, 1991). Since in a slurry bubble-column axial pressure drop is due to hydrostatic pressure, in an unloaded system gas holdups could be determined from the readings on the central pressure indication points. Gas holdups determined at 29°C for gases with different molar masses (He, N_2, SF_6) showed the expected trend. Thus it seems probable that in our setup bubble diameter is also influenced by the molar mass of the gas. We did not, however, find any effect of the molar mass of the gas on the filtration behavior observed in our system (Figure 14). From this we can conclude that the bubble diameter is of no importance to the filtration hydrodynamics in our column.

Influence of Load of Solids

In Figures 12 and 13 the influence of the load of solids on the experimentally determined and theoretically calculated cake ratio curves is shown. The gas velocity used in the cake buildup number has been corrected for cross-sectional area reduction due to cake formation (Eq. 22). For the unknown constants in both models (i.e., C_σ and α) the values obtained by fitting to results for a 15-g load were used. It follows both from experiments and from theory that the cake ratio for a certain value of the cake buildup number increases with the load of particles.

If it is assumed that the total mass of solids in the bulk is directly proportional to its concentration at the axial position of the filter, both the surface-renewal model and the force-balance model predict that at each value of the cake buildup number there exists a certain equilibrium content of solids in the bulk that is independent of the load of solids in the system. Further assuming that cake resistance is directly proportional to cake volume, cake ratio can be seen as the volume fraction of the particles present in a system that is part of the cake. It then follows from a mass balance:

$$\text{CR} = 0: \qquad V^* \geq \frac{M_{s,\text{tot}}}{\rho_s}$$

$$\text{CR} > 0: \qquad V^* = (1 - \text{CR}) \frac{M_{s,\text{tot}}}{\rho_s}. \tag{27}$$

The first part of the preceding equation indicates that as long as there are no particles in the cake, the bulk can at least contain the volume of solids present in the system. If

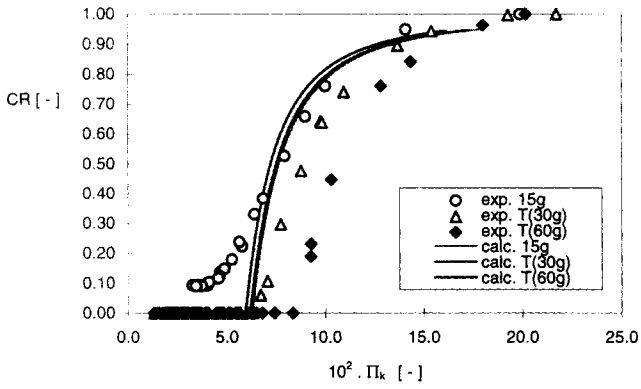

Figure 15. Effect of mass-balance-based load transformation (Eq. 28) on experimental and surface-renewal model ($C_\sigma = 1.40$) results.

The dimensionless number has been corrected for cross-sectional area reduction (Eq. 22): $d_p = 96$ μm, $T = 29$°C, gas = N_2.

there are particles present in the cake, the bulk of the system exactly contains its equilibrium content, as presented by the second part of Eq. 27. The equilibrium content of solids at a certain value of the cake buildup number, as calculated from the preceding equation for a certain load of particles, can now be used to obtain the cake ratio at the same cake buildup number at any lower load. After some rearrangement, this leads to:

$$M_{s,\mathrm{tot,I}} \geq M_{s,\mathrm{tot,II}}:$$

$$\mathrm{CR_I} \leq 1 - \frac{M_{s,\mathrm{tot,II}}}{M_{s,\mathrm{tot,I}}}: \qquad \mathrm{CR_{II}} = 0$$

$$\mathrm{CR_I} > 1 - \frac{M_{s,\mathrm{tot,II}}}{M_{s,\mathrm{tot,I}}}: \qquad \mathrm{CR_{II}} = 1 - (1 - \mathrm{CR_I})\,\frac{M_{s,\mathrm{tot,I}}}{M_{s,\mathrm{tot,II}}}. \tag{28}$$

Using the preceding equation cake ratio curves for a certain load of particles can be predicted from results at an arbitrary higher load. It can be seen from Figure 15 that the transformation performs quite well within the framework of the surface-renewal model. Similar results for the force-balance model are not shown here, since the transformed curves lie almost on top of each other. The remaining deviation can be explained on the basis of an effect of liquid velocity. At a certain superficial gas velocity, the gas velocity in the filter zone is higher at a higher load of solids due to the fact that a part of the available cross-sectional area is blocked by the cake present. Therefore at the same cake buildup number permeate flux and liquid velocity are higher, leading to a reduction of solids volume in the bottom zone and an increase in cake volume and ratio.

The experimental results show the inverse trend as compared to theory. This may be due to the presence of the residual resistance on the left of the curves, which is not predicted from theory. Another effect that may have influenced the shape of the curve is particle-size distribution (PSD). Even though particles with a narrow size distribution have been used, they still possess a certain amount of polydispersity. Therefore the particles responsible for the final quarter of the resistance of 60 g of glass beads may be significantly larger than the particles present in 15 g of glass beads. On the other hand, their concentration will be higher since specific resistance is inversely proportional to particle diameter squared (Eq. 18). If the effect of increased diameter to be substituted in the dimensionless number outbalances the influence of concentration increase, model predictions will indicate the same qualitative trend with respect to the influence of the load, as the measurements do. Effects of PSD on equilibrium at the axial position of filters and axial solids distribution are the subject of further study.

Conclusion

For internal filtration in slurry bubble columns, a novel dimensionless number has been derived on the basis of two different theoretical approaches. The resulting models predict that this dimensionless number uniquely determines the solids bulk holdup at the axial position of the filter. Experiments in which the resistance of the filter cake was determined as an indirect measure of solids concentration have proven the validity of the novel dimensionless number. Theory and experiment do differ, however, with respect to the shape of the measured curves and the influence of the load of solids. These discrepancies may be partly attributed to the neglect of the influence of particle-size distribution in both model types.

The characteristic length scale of the resuspending eddies in our system corresponds to the Kolmogoroff length scale. For resuspension in stirred tanks and in slurry pipe flow, the characteristic length scale of the resuspending eddies equals the particle diameter. In our system particle diameter and Kolmogoroff length scale are of the same order of magnitude (which is quite common in slurry bubble columns), while in the other cases particle size significantly exceeded the Kolmogoroff length scale. The ratio of particle size and Kolmogoroff length scale therefore appears to determine the length scale of the eddies responsible for particle resuspension.

Acknowledgments

These investigations were supported by the Dutch Research School for Process Technology (O.S.P.T.). The authors also acknowledge W. Leppink for his technical support, J. C. Bosma and C. van Gulijk for their part in the theoretical work, and M. G. Eltink for his contribution to the experimental work.

Notation

a_b = slurry fraction of the cross-sectional area in the filter zone
C_τ = proportionality constant in the surface-renewal model
$D_{\mathrm{ax,s}}$ = solids axial dispersion coefficient, $\mathrm{m^2 \cdot s^{-1}}$
d_h = hydraulic column diameter, m
g = gravitational force per unit mass, $\mathrm{m \cdot s^{-2}}$
L = width of a filter plate, m; depth of column, m
$\bar{R}_c$ = specific cake resistance, $\mathrm{m^{-2}}$
t = time, s
V_k = Kolmogoroff velocity scale, $\mathrm{m \cdot s^{-1}}$
V_t = terminal velocity of a single particle in a stagnant fluid, $\mathrm{m \cdot s^{-1}}$
V^s = volume of solids, $\mathrm{m^3}$
V^* = volume of solids present in the bulk at hydrodynamic equilibrium, $\mathrm{m^3}$
W = distance between filter plates, m; width of column, m
x = radial distance from filter cake, m
z = axial coordinate, m

Dimensionless numbers

$Fr_g = U_g/\sqrt{(gd_h)}$, Froude number
$Pe_s = U_g d_h/D_{ax,s}$, Peclet number
$Re_t = v_t d_p/\nu_l$, particle terminal Reynolds number

Greek letters

Δp = pressure drop, $kg \cdot m^{-1} \cdot s^{-2}$
ϵ_g = volume fraction of gas; 1 − (volume fraction of slurry)
ϵ_s = volume fraction of solids in slurry; 1 − (volume fraction of liquid in slurry)
η = dynamic viscosity, $kg \cdot m^{-1} \cdot s^{-1}$
ρ = density, $kg \cdot m^{-3}$
ω = surface tension, $kg \cdot s^{-2}$

Subscripts and superscript

b = bulk property
k = Kolmogoroff
p = particle
tot = total
$*$ = hydrodynamic equilibrium

Literature Cited

Beenackers, A. A. C. M., and W. P. M. van Swaaij, "Mass Transfer in Gas-Liquid Slurry Reactors," *Chem. Eng. Sci.*, **48**, 3109 (1993).

Chapman, B. K., and D. T. Leighton, Jr., "Dynamic Viscous Resuspension," *Int. J. Multiphase Flow*, **17**, 469 (1991).

Cova, D. R., "Catalyst Suspension in Gas-Agitated Tubular Reactors," *Ind. Eng. Chem. Proc. Des. Dev.*, **5**, 20 (1966).

Darton, D. C., "Hydrodynamics, Heat and Mass Transfer in Three-Phase Fluidized Beds," *Proc. ICHMT Symp. Heat and Mass Transfer in Fixed and Fluidized Beds*, Dubrovnik, Yugoslavia (1984).

Davies, J. T., *Turbulence Phenomena*, Academic Press, New York (1972).

Davies, J. T., "Particle Suspension and Mass Transfer in Agitated Vessels," *Chem. Eng. Proc.*, **20**, 175 (1986).

Davies, J. T., "Calculation of Critical Velocities to Maintain Solids in Suspension in Horizontal Pipes," *Chem. Eng. Sci.*, **42**, 1667 (1987).

Davis, R. H., "Theory for Crossflow Microfiltration," *Membrane Handbook*," Chap. 33, W. S. Ho and K. K. Sirkar, eds., van Nostrand Reinhold, New York (1992).

Deckwer, W. D., "On the Mechanism of Heat Transfer in Bubble Column Reactors," *Chem. Eng. Sci.*, **35**, 1341 (1980).

Deckwer, W. D., Y. Louisi, A. Zaidi, and M. Ralek, "Hydrodynamic Properties of the Fischer-Tropsch Slurry Process," *Ind. Eng. Chem. Proc. Des. Dev.*, **19**, 699 (1980).

Deckwer, W. D., and A. Schumpe, "Blasensäulen—Erkenntnisstand und Entwicklungstendenzen," *Chem. Ing. Tech.*, **57**, 754 (1985).

Hinze, J. O., *Turbulence* 2nd ed., McGraw-Hill, New York (1975).

Ishida, H. Y., Yamada, M. Tsuboi, and S. Matsumura, "Submerged Membrane Activated Sludge Process (KSMASP)—Its Application into Activated Sludge Process with High Concentration of MLSS," Int. Conf. on Advances in Water and Effluent Treatment, Cumbria (United Kingdom) (1993).

Jager, B., A. P. Steynberg, J. R. Inga, R. C. Kelfkens, M. A. Smith, and F. E. J. Malherbe, "Process for Producing Liquid and, Optionally Gaseous Products from Gaseous Reactants," Sasol Chemical Industries Ltd., Johannesburg, South Africa, EP 0 0609 079 A1 (1994).

Kato, Y., A. Nishiwaki, T. Fukuda, and S. Tanaka, "The Behavior of Suspended Solid Particles and Liquid in Bubble Columns," *J. Chem. Eng. Jpn.*, **5**, 112 (1972).

Kraft, A., and U. Mende, "Niedrigenergie-Membranverfahren zum Biomassenrückhalt in Abwasserreinigungsanlagen," *Filtr. Sep.*, **9**, 245 (1995).

Kuboi, R., I. Komasawa, and T. Otake, "Behavior of Dispersed Particles in Turbulent Liquid Flow," *J. Chem. Eng. Jpn.*, **5**, 349 (1972).

Leighton, D., and A. Acrivos, "Viscous Resuspension," *Chem. Eng. Sci.*, **41**, 1377 (1986).

Rytter, E., P. Roterud, P. Lian, and T. Myrstad, "Solid-Liquid Slurry Treatment Apparatus and Catalytic Multi-Phase Reactor," *Den Norske Stats Oljeselskap A.S., Stavanger (Norway), WO 94/16807 (1994).*

Wen, C. Y., and Y. H. Yu, "Mechanics of Fluidization," *Chem. Eng. Prog. Symp. Ser.*, **62**, 100 (1966).

Wilkinson, P. M., "Physical Aspects and Scale-Up of High Pressure Bubble Columns," PhD Thesis, Univ. of Groningen, Gronigen, The Netherlands (1991).

Appendix

In this Appendix a limiting solution to the surface-renewal model and an analytical expression for the penetration depth of the solids are derived.

Suppose that at hydrodynamic equilibrium a fully developed concentration profile is established at the end of the stay of the liquid packets at the cake surface. In this situation the time derivative can be neglected in Eq. 4, and the resulting ordinary differential equation can be substituted in the equilibrium condition (Eq. 8) to yield

$$\frac{J}{d_p}\sqrt{\frac{\nu_l}{U_g g}} = \frac{1}{2}\sqrt{\frac{C_\sigma}{C_\tau}}\sqrt{\frac{\rho^*_{sl,b}}{\rho_l}}\,\frac{1-\epsilon^*_{s,b}}{\sqrt{\epsilon^*_{s,b}\,\epsilon_{s,c}}}\sqrt{I_1} \tag{A1}$$

$$I_1 = \frac{1}{3}\epsilon_c\left(\epsilon_c^3 - \epsilon_b^3\right) - \frac{1}{4}(1+\epsilon_c)\left(\epsilon_c^4 - \epsilon_b^4\right) + \frac{1}{5}\left(\epsilon_c^5 - \epsilon_b^5\right)$$

$$\epsilon_b = \epsilon^*_{s,b}; \qquad \epsilon_c = \epsilon_{s,c}.$$

Numerical solution of the nonstationary nonlinear diffusion equation (Eq. 4) using a discretization technique showed that the preceding analytical expression describes the computational result within an error of 0.4% for solidities up to 10 vol. %. For higher solids concentrations only the part depending on the solids holdup needs to be modified to describe the numerical solution accurately.

In the preceding derivations a continuum approach is followed, which is, strictly speaking, only valid if penetration depth is considerably larger than particle diameter. For low solids concentrations an analytical expression for the former can be derived. Again neglecting the time derivative in Eq. 4 the following implicit expression can be obtained for the solids concentration profile in the liquid element:

$$\frac{x}{d_p} = \left(\frac{\eta^*_{sl,b}\,\rho^*_{sl,b}}{\eta_l\,\rho_l}\right)^{1/2}\frac{1}{4}C_\sigma\frac{1}{\Pi_{sr}}\,\frac{1-\epsilon^*_{s,b}}{\epsilon_{s,c}}\,I_2 \tag{A2}$$

$$I_2 = \frac{1}{4}\left(\epsilon_{s,c}^4 - \epsilon_s^4\right) + \frac{1}{3}\left(\epsilon^*_{s,b} - 1 - \epsilon_{s,c}\right)\left(\epsilon_{s,c}^3 - \epsilon_s^3\right)$$

$$+\left(\epsilon_{s,c} + \epsilon^*_{s,b}\left(\epsilon^*_{s,b} - 1 - \epsilon_{s,c}\right)\right) I_3$$

$$I_3 = \frac{1}{2}\left(\epsilon_{s,c}^2 - \epsilon_s^2\right) + \epsilon^*_{s,b}\left(\epsilon_{s,c} - \epsilon_s\right) + \epsilon^{*2}_{s,b}\ln\left(\frac{\epsilon_{s,c} - \epsilon^*_{s,b}}{\epsilon_s - \epsilon^*_{s,b}}\right).$$

Defining penetration depth as the distance from the cake at which the driving force for diffusion is reduced to 1 % of its value at the cake surface, it follows that

$$\frac{x}{d_p} \approx \left(\frac{\eta^*_{sl,b}\,\rho^*_{sl,b}}{\eta_l\,\rho_l}\right)^{1/2}\frac{1}{4}C_\sigma\frac{1}{\Pi_{sr}}\,0.05. \tag{A3}$$

Manuscript received May 27, 1997, and revision received Jan. 30, 1998.